Multidimensional terahertz probes of quantum materials

Check for updates

Albert Liu ✉

Multidimensional spectroscopy has a long history originating from nuclear magnetic resonance, and has now found widespread application at infrared and optical frequencies as well. However, the energy scales of traditional multidimensional probes have been ill-suited for studying quantum materials. Recent technological advancements have now enabled extension of these multidimensional techniques to the terahertz frequency range, in which collective excitations of quantum materials are typically found. This Perspective introduces the technique of two-dimensional terahertz spectroscopy (2DTS) and the unique physics of quantum materials revealed by 2DTS spectra, accompanied by a selection of the rapidly expanding experimental and theoretical literature. While 2DTS has so far been primarily applied to quantum materials at equilibrium, we provide an outlook for its application towards understanding their dynamical non-equilibrium states and beyond.

The physics of quantum materials is one of the frontiers of modern condensed matter physics[1]. It presents a broad, formidable challenge, in particular due to the interaction of numerous degrees of freedom and their dynamical fluctuations, yet resolving these microscopic physics promises an unprecedented understanding of these quantum materials. How quantum materials cross phase boundaries in equilibrium, and how they are driven into new phases of matter with no equilibrium counterpart are questions essential to realizing their imaginable functionalities[2,3].

To this end, important messengers of the underlying physics are changes in their excitation spectra that accompany structural and electronic rearrangements, which typically occur in the terahertz (10^{12} Hz) frequency range[4,5]. Yet our understanding and exploitation of material properties in the terahertz frequency range has been hindered by the challenges of generating, detecting, and manipulating light at these frequencies[6] for spectroscopic applications. In particular, many aspects of coupling between different degrees of freedom, complex many-body interactions, and dynamical phenomena remain hidden in conventional terahertz spectroscopies[7–9] sensitive only to two-point correlations of relevant observables.

In contrast, sophisticated techniques have been developed at microwave frequencies for nuclear magnetic resonance (NMR) spectroscopy[10,11] to access higher-order correlations of spin degrees of freedom. Various excitation schemes are routinely used to distill material nonlinearities, and have also been translated to the visible and near-infrared frequency ranges[12,13]. In particular, multidimensional coherent spectroscopy at optical frequencies[14] has emerged as the preeminent method for disentangling complex electronic dynamics in chemical and biological systems[15], allowing spectroscopists to dissect material nonlinearities into their individual constituent terms[16].

Significant efforts have now been made to extend multidimensional techniques into the terahertz frequency range towards two-dimensional terahertz spectroscopy (2DTS)[17]. Since its first demonstration over a decade ago[18], the growing accessibility of strong-field terahertz light sources has led to applications of 2DTS in a wide variety of material systems[19–30]. But perhaps their most intriguing applications lie in quantum materials, whose spectacular emergent properties arise precisely from the electronic correlations that 2DTS excels at resolving. In this Perspective, we introduce 2DTS as a powerful new technique for studying the intrinsic properties of quantum materials and discuss future opportunities for applying 2DTS as an ultrafast probe of quantum materials dynamically driven out of equilibrium with light[31].

Basics of 2-D terahertz spectroscopy

The basics of 2-D spectroscopy at infrared and optical frequencies are well-established and has been described extensively in the literature from a quantum level-system perspective[12,13]. On the contrary, low-energy collective excitations of quantum materials are often described by effective coordinates and their equations of motion[4]. Our starting point will therefore be the generic potential energy of a coordinate x, which takes the form:

$$U(x) = \frac{1}{2}\omega_0^2 x^2 + z^* x E(t) + U_{anh} \qquad (1)$$

where ω_0 is its resonance frequency dictated by the harmonic potential and z^* is the effective charge that determines dipolar coupling of the coordinate to an external time-dependent electric field $E(t)$. In the following we provide a brief introduction to the nonlinearities of a classical oscillator and their
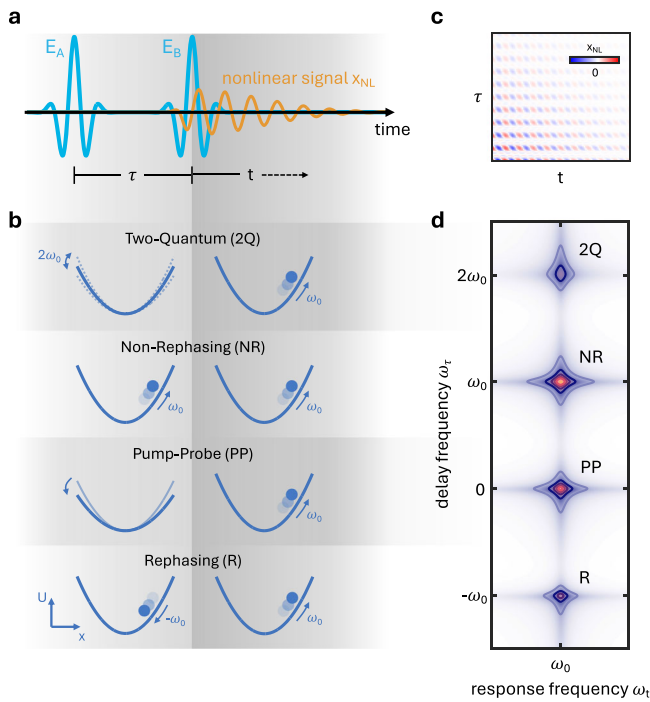

Condensed Matter Physics and Materials Science Division, Brookhaven National Laboratory, Upton, NY, 11973, USA. ✉e-mail: aliu1@bnl.gov

Fig. 1 | Classical view of two-dimensional terahertz spectroscopy. a Terahertz excitation pulse sequence involving two nominally identical fields E_A and E_B separated by a time delay τ. A nonlinear signal x_{NL} then evolves along the real laboratory time t. **b** Illustrations of the four third-order nonlinearities with a response frequency of ω_0 that result from a soft quartic anharmonicity. Note that the two remaining third-harmonic generation nonlinearities occur, but are not shown here. **c** Nonlinear signal x_{NL} in the time-domain as a function of $\{\tau, t\}$, which exhibits intricate oscillatory behavior due to interference between the multiple nonlinearities. **d** Fourier transform of the time-domain signal in **c**, showing four distinct peaks corresponding to the four nonlinearities illustrated in **b** as indicated.

corresponding 2-D spectra, which will then lend intuition to the unique physics underlying various features that we describe later.

Self-anharmonicity

As a heuristic example, we take a quartic potential nonlinearity of the form:

$$U_{anh}(x) = -\frac{1}{4}ax^4, \tag{2}$$

where a is an anharmonic coefficient that determines the strength of the nonlinearity. We will assume the case of a 'soft spring' ($a > 0$), which describes, for example, the Josephson plasma resonance in layered superconductors[32–34].

In its most common realization, 2DTS involves two identical terahertz excitation pulses (denoted E_A and E_B) that cooperatively drive a nonlinear response of the coordinate (shown in Fig. 1a). This nonlinear signal is then generically a function of two variables, the inter-pulse time delay τ and the real laboratory time t that evolves following interaction with the second pulse E_B. In the harmonic oscillator limit ($a = 0$), the superposition principle dictates that the coordinate response to $E_A + E_B$ is simply the summation of the individual responses to E_A and E_B alone. With the nonlinearity included however, the superposition principle is broken by a displacement-dependent resonance frequency[35]

$$\omega^2(x) = \omega_0^2 - ax^2. \tag{3}$$

Despite the simple nature of the underlying quartic potential, an infinite hierarchy of nonlinear coordinate responses scaling with $E_A^n E_B^m$ (where $n + m$ is odd) results to arbitrary order[36]. Here we will only consider the most

commonly measured third-order ($n + m = 3$) coordinate response composed of six contributing nonlinearities, four that emit at the fundamental resonance frequency ω_0 and two that emit at triple its value $3\omega_0$ (third-harmonic generation). We further restrict our focus to only the four former terms, as the third-harmonic nonlinearities typically contain redundant information[34].

To interpret such impulsive nonlinearities, it is most natural to consider the dynamics driven by E_A and E_B sequentially. Beginning with the arrival of E_A, its interaction with the system results in two primary consequences for the subsequent interaction with E_B a time τ later (illustrated in Fig. 1b). First, it can immediately be seen from (3) that the resonance frequency is both rectified and modulated at twice the resonance frequency $2\omega_0$[37]. Second, E_A introduces a time-dependent initial condition that either enhances or suppresses the response to E_B (beyond a simple superposition of the two individual responses). To emphasize, these nonlinearities occur simultaneously and share a common response frequency $\omega_t = \omega_0$, resulting in overlapping signatures in one-dimensional spectra. As will be shown in the following however, this ambiguity is lifted in a two-dimensional spectrum.

Two-dimensional spectrum

To isolate the nonlinearities cooperatively driven by both E_A and E_B from their individual responses, one measures a nonlinear signal defined by

$$x_{NL}(\tau, t) = x(\tau, t)|_{Aon,Bon} - x(\tau, t)|_{Aon,Boff} - x(\tau, t)|_{Aoff,Bon}. \tag{4}$$

The equation of motion resulting from (2) may be straightforwardly solved[36] as a function of $\{\tau, t\}$ to obtain $x_{NL}(\tau, t)$, which exhibits complex oscillatory dynamics along both time axes as shown in Fig. 1c. Interpretation of these dynamics is difficult in the time-domain, but becomes tractable in the frequency-domain. To this end, two-dimensional Fourier transform of $x_{NL}(\tau, t)$ correlates the dynamics along τ and t in a two-dimensional (2-D) spectrum shown in Fig. 1d.

In the two-dimensional (2-D) spectrum, four peaks appear at a response frequency $\omega_t = \omega_0$, corresponding to the four nonlinearities described above. Two peaks appear at delay frequencies $\omega_\tau = 0$ and $\omega_\tau = 2\omega_0$, corresponding to rectification and parametric modulation of the resonance frequency, and are denoted the 'Pump-Probe' and 'Two-Quantum' peaks respectively. The two other peaks appearing at $\omega_\tau = \omega_0$ and $\omega_\tau = -\omega_0$ then arise from in-phase or out-of-phase modulation (by the first excitation pulse E_A) of the nonlinear signal (stimulated by the second excitation pulse E_B), and are denoted the 'non-rephasing' and 'rephasing' peaks respectively. These nonlinearities, illustrated in Fig. 1b and designated with terminology borrowed from atomic and molecular physics[12,13], are summarized in Table 1 along with their excitation field scaling (in terms of positive and negative frequency components $E_{A/B}e^{i\omega t}$ and $E_{A/B}^*e^{-i\omega t}$) and frequency coordinates. We emphasize that, despite the apparent simplicity of (2), these spectral features are generic for the third-order nonlinearity of an anharmonic oscillator and bear direct correspondence to their quantum level system counterparts. The classical description of their underlying mechanisms described here then lends intuition to how the various physics of quantum materials manifest in different features of a 2DTS spectrum, which will be the focus of the following section.

2DTS of quantum materials: in equilibrium

In the previous section, we considered an anharmonic oscillator whose nonlinearity derives solely from a quartic potential nonlinearity. While instructive, this model can never realistically capture the physics of quantum materials. For example, collective excitations in real solids are dispersive, are affected by thermal fluctuations, couple to other degrees of freedom, and can suffer from material disorder. While such complications are difficult to disentangle with conventional spectroscopic probes, their effects naturally separate into unique features in a 2-D spectrum.

Table 1 | Third-order wave-mixing nonlinearities

Signal	Dependence	(ω_τ, ω_t)
Two-Quantum (2Q)	$E_A^2 E_B^* e^{i\omega_0(2\tau+t)}$	$(2\omega_0, \omega_0)$
Non-Rephasing (NR)	$E_A |E_B|^2 e^{i\omega_0(\tau+t)}$	(ω_0, ω_0)
Pump-Probe (PP)	$|E_A|^2 E_B e^{i\omega_0 t}$	$(0, \omega_0)$
Rephasing (R)	$E_A^* E_B^2 e^{i\omega_0(t-\tau)}$	$(-\omega_0, \omega_0)$
Third-Harmonic 1 (3H1)	$E_A^2 E_B e^{i\omega_0(3t+2\tau)}$	$(2\omega_0, 3\omega_0)$
Third-Harmonic 2 (3H2)	$E_A E_B^2 e^{i\omega_0(3t+\tau)}$	$(\omega_0, 3\omega_0)$

Different peaks, different physics

In 2-D spectra of quantum materials, different aspects of their microscopic physics distort specific peaks away from their generic forms shown in Fig. 1d. Examples of such phenomena are illustrated in Fig. 2 and summarized below for each peak.

Two-quantum (2Q). The two-quantum nonlinearity, as its name suggests, tracks dynamics evolving at (or near) twice the excitation photon frequency. These dynamics may arise classically, for example from parametric modulation of the resonance frequency (as illustrated in Fig. 1b). They may also be of quantum mechanical origin, arising from quantum coherences between two quasiparticle excitations and an unoccupied ground state[38]. Such two-quantum nonlinearities have been observed, for example, for magnetic excitations in orthoferrites[39,40] and Josephson plasmons in layered cuprates[28]. In quantum materials, the two-quantum nonlinearity is particularly important for probing material anharmonicities[41], which can result in bound states of collective excitations such as bimagnons[42] or biphonons[43]. As illustrated in Fig. 2, for a binding energy $\hbar\delta$ exceeding the resonance linewidth, the two-quantum nonlinearity (1) shifts vertically along ω_τ by δ and (2) splits horizontally along ω_t into two peaks separated by δ. The two resultant peaks then correspond to a transition back into the unoccupied ground state ($\omega_t = \omega_0$) and dissociation of the collective bound state into single quasiparticles ($\omega_t = \omega_0 - \delta$).

Non-rephasing (NR). The non-rephasing nonlinearity is the strongest nonlinearity for a classical anharmonic oscillator, as in-phase excitation between E_A and E_B cooperatively drive the coordinate to the largest amplitude (strongest effect of anharmonicity). Besides its role in generating absorptive 2-D spectra (useful when conventional 2-D spectra are congested with overlapping peaks[44]), the non-rephasing nonlinearity is also sensitive to fluctuating order. In a recent theoretical study, Salvador et al. have predicted[34] non-rephasing 2-D spectra of the Josephson plasma resonance to contain signatures of superconducting fluctuations. To see this, one must consider a nonlinear excitation process (beyond the mean-field approximation) illustrated in the top right panel of Fig. 2, in which two electric field interactions drive pairs of finite-momentum plasma waves at equal and opposite momenta[45]. In the corresponding non-rephasing 2-D spectrum, a symmetric peak is observed whose peak position is fixed by the driving frequency ($\omega_\tau, \omega_t) = (\omega_d, \omega_d)$ due to energy conservation. This is in stark contrast to the spectrum predicted by mean-field theory for a damped oscillator, which exhibits a peak whose lineshape directly follows the linear loss function[34] (centered at the plasma frequency ω_0). We anticipate the non-rephasing nonlinearity to also be sensitive to analogous processes of other types of excitations such as Klemens decay of phonons[46] or 3-magnon scattering[47].

Pump-probe (PP). As evidenced by its scaling with $|E_A|^2$, independent of excitation phase, the pump-probe nonlinearity encompasses all incoherent (non-oscillatory) dynamics. Perhaps the most ubiquitous of such nonlinearities are thermal effects, in which initial excitation by E_A (typically) raises the electronic temperature to a transient, non-
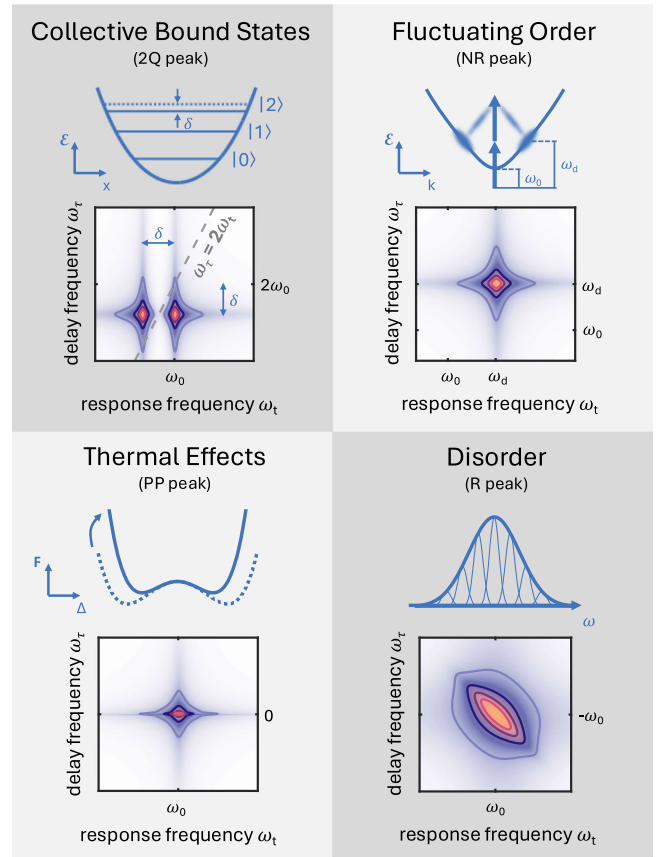

Fig. 2 | The unique physics of quantum materials revealed by each peak. Top left: The two-quantum (2Q) nonlinearity probes doubly-occupied states of a quantum oscillator, and exhibits unique signatures of quasiparticle bound states of binding energy δ. Top right: The non-rephasing (NR) nonlinearity is sensitive (though not uniquely) to finite-momentum fluctuations, resulting in a peak position determined by the driving frequency ω_d rather than the resonance frequency ω_0. Bottom left: The pump-probe (PP) nonlinearity captures all incoherent (non-oscillatory) processes. Most notably all thermal effects are isolated in this peak, leaving only non-thermal coherent dynamics elsewhere in the 2-D spectrum. Bottom right: The rephasing nonlinearity is unique in its sensitivity to disorder. In the absence of disorder the rephasing peak is symmetric while in the presence of disorder the rephasing peak elongates as shown.

equilibrium value. The bottom left panel of Fig. 2 illustrates such a thermal nonlinearity for an ordered system, in which the free energy is thermally-quenched by optical excitation. The corresponding pump-probe 2-D spectrum then exhibits a narrow lineshape along the vertical ω_τ axis, reflecting the long timescales of thermal relaxation processes. A recent experiment by Kim et al. on the cuprate superconductor $La_{2-x}Sr_xCuO_4$[48] exploited this ability of 2DTS to separate coherent and incoherent dynamics, observing a strong pump-probe nonlinearity due to incoherent breaking of Cooper pairs[49] that is spectrally separated from the coherent order parameter dynamics. We note that in the case of dominant incoherent optical processes (thermal or otherwise) the pump-probe nonlinearity will appear alone in 2-D spectra, which has been observed in varied systems[24,26,50,51].

Rephasing (R). The rephasing nonlinearity is most well-known for its usefulness in studying disorder (being responsible for optical photon echoes[52] and spin echoes in nuclear magnetic resonance[53]), which may be understood from either a time- or frequency-domain perspective for a disordered ensemble of oscillators (valid in the limit of strong localization). In the time-domain, the first pulse E_A coherently excites dynamics of the ensemble which dephase due to disorder, obscuring their intrinsic
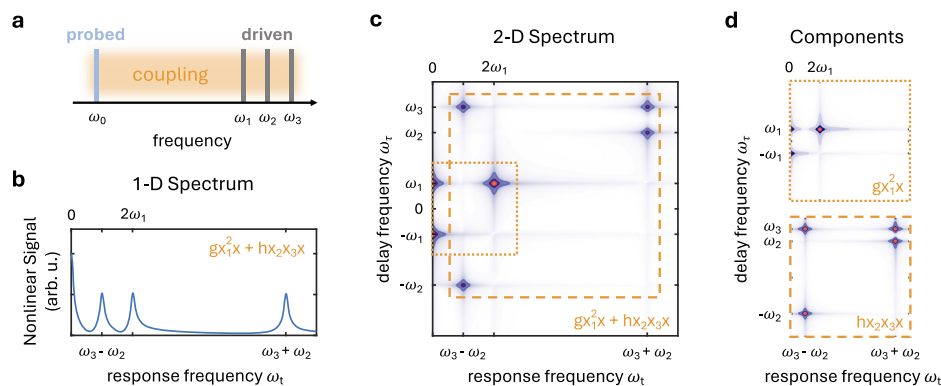
Fig. 3 | Dissecting anharmonic coupling using 2DTS. a Depiction of the probed coordinate x with a resonance frequency ω_0 indirectly excited through coupling to three driven modes $\{x_1, x_2, x_3\}$ with resonance frequencies $\{\omega_1, \omega_2, \omega_3\}$. Schematic **b** one-dimensional and **c** two-dimensional spectra of the nonlinear response resulting from the total anharmonic coupling $U_{anh} = gx_1^2 x + hx_2 x_3 x$. The one-dimensional spectrum exhibits peaks at various response frequencies ω_t that are ambiguous to the underlying coupling mechanisms, while the 2-D spectrum provides more intricate peak patterns that inform the underlying drive frequencies. **d** Decomposition of the total spectrum shown in **c** into its two constituent components, which exhibit characteristic peak patterns used to identify the coupling term responsible. Note that the schematic spectra shown in **b**–**d** are obtained under a driven condition, in which the nonlinear driving force exceeds the oscillation period of x. In the inverse condition, impulsive excitation of x becomes possible and additional features along $\omega_t = \omega_0$ appear.

lifetime. Arrival of the second pulse E_B then performs a time-reversal operation, reversing the extrinsic dephasing and 'rephasing' the ensemble after a time $t = \tau$. The bottom right panel of Fig. 2 then illustrates the frequency-domain perspective with both a 1-D spectrum and rephasing 2-D spectrum. In the 1-D spectrum, the resonance lineshape is broadened by a combination of both intrinsic and extrinsic broadening and one cannot disentangle the two effects. In the 2-D spectrum, these two broadening mechanisms are projected into orthogonal directions and produce an asymmetric 'almond' peak shape[34,54,55]. Recent 2DTS experiments have exploited this rephasing nonlinearity to measure intrinsic linewidths in doped silicon[23] and to characterize disordered superconductivity in the cuprate $La_{2-x}Sr_xCuO_4$[28]. Analogous theoretical proposals have also been put forth toward resolving fractional excitations in spin liquids[56,57].

Beyond third-order nonlinearities

The third-order nonlinearities described above typically capture the most prominent features observed in 2DTS experiments. However, the intense excitation employed in many 2DTS experiments, with peak electric fields in the kV/cm to MV/cm range, can drive even higher-order nonlinearities which have been observed in various systems.

An early example of such high-order nonlinearities in 2DTS spectra was reported by Maag et al. on magnetically-biased quantum wells[20]. With application of a magnetic field, the energies of the electron gas are quantized to Landau levels whose resonance frequencies are independent of electron-electron interactions - the celebrated theorem by Kohn[58]. Kohn's theorem can be violated, however, by intense terahertz excitation. The physical mechanisms responsible were then clarified using 2DTS, which differed depending on excitation regime. At the lowest excitation fields, third-order nonlinearities dominate the 2DTS spectra and are due to band non-parabolicities. With stronger excitation fields however, fifth-order nonlinearities appear and the nonlinear optical response is determined by Coulomb effects between the electron gas and ionic background.

Recently, Huang et al. accessed an even more remarkable regime in 2DTS of the orthoferrite $Sm_{0.4}Er_{0.6}FeO_3$[40]. With driving fields in the MV/cm regime, features appear in 2DTS spectra that arise from magnon nonlinearities up to sixth-order, including fourth-, fifth-, and sixth-harmonic generation. The 2DTS spectra were only reproduced by simulations including both four-fold magnetic anisotropy and the Dzyaloshinskii-Moriya interaction, which underscores the exquisite sensitivity of high-order 2DTS spectra to the subtle physics of complex magnetic systems.

Coupled resonances

At this point we have considered only a single driven oscillator and its self-anharmonicities[59]. In real quantum materials however, anharmonic coupling between different resonances plays an essential role in their material properties and is also responsible for many of their most intriguing behaviors[60]. Such coupling is intricate, usually involving many degrees of freedom, and is difficult to decipher with one-dimensional spectroscopies. Disentangling the underlying coupling mechanisms in quantum materials is therefore a primary application of 2DTS, as we will demonstrate in the following.

As an example, we consider lowest-order anharmonic coupling (in a centro-symmetric system) between a coordinate x and three coupled coordinates $\{x_1, x_2, x_3\}$, namely quadratic-linear[61] and tri-linear[62] coupling of the form:

$$U_{anh}(x_1, x_2, x_3, x) = gx_1^2 x + hx_2 x_3 x \qquad (5)$$

where g and h are the anharmonic coefficients and the coupled coordinates $\{x_1, x_2, x_3\}$ have resonance frequencies $\{\omega_1, \omega_2, \omega_3\}$ respectively. Symmetry considerations then require the coordinates $\{x_1, x_2, x_3\}$ to be infrared-active and the common coordinate x to be Raman-active ($z^* = 0$). As illustrated in Fig. 3a, $\{x_1, x_2, x_3\}$ are directly driven by the excitation fields while the common coordinate x is indirectly driven by anharmonic coupling and the corresponding force

$$F_x(x_1, x_2, x_3) = -\frac{\partial U_{anh}}{\partial x} = -gx_1^2 - hx_2 x_3, \qquad (6)$$

where the former term gives rise to both a rectified ($\omega = 0$) and second-harmonic ($\omega = 2\omega_1$) response while the latter term results in sum/difference frequency ($\omega = \omega_3 \pm \omega_2$) responses.

In the most general one-dimensional measurement of coupling in this system, an initial pulse resonantly excites all three coordinates $\{x_1, x_2, x_3\}$ before a subsequent pulse measures the response of x via an observable such as transient reflectivity or transient birefringence. We further assume a driven condition, in which the nonlinear driving force exceeds the oscillation period of x. As shown in Fig. 3b, the resultant one-dimensional measurement yields, however, only the response frequencies while providing minimal information on the underlying coupling mechanisms.

In contrast, the corresponding 2-D spectrum shown in Fig. 3c is far richer. In addition to the response frequency axis, the dynamics are now spectrally resolved along the delay frequency axis ω_τ to produce two-dimensional peak structures characteristic of specific coupling mechanisms.

In Fig. 3c, two sets of peaks (outlined by the dotted and dashed boxes) can be identified as corresponding to the two coupling terms in (5). The peak pattern of each component, plotted individually in Fig. 3d, may then be intuitively understood by considering their coordinates along the two frequency axes ω_τ and ω_t.

Given a set of peaks at a particular response frequency ω_t, their corresponding coordinates along the delay frequency ω_τ indicate the parent driving frequencies that derive from (6). This may be most easily understood in the spectrum of $U_{anh} = hx_2x_3x$ (bottom panel of Fig. 3d), where two peaks at $\omega_t = \omega_3 + \omega_2$ appear at corresponding delay frequencies $\omega_\tau = + \omega_3$ and $\omega_\tau = + \omega_2$ that unambiguously indicate a sum-frequency generation process. The two peaks at $\omega_t = \omega_3 - \omega_2$ likewise appear at $\omega_\tau = \omega_3$ and $\omega_\tau = -\omega_2$ to indicate a difference-frequency generation process. These fingerprints of sum- and difference-frequency generation processes were recently observed, for example, between magnon modes in $YFeO_3$[63].

The spectrum of $U_{anh} = gx_1^2x$ (top panel of Fig. 3d) (which can be intuited as the $U_{anh} = hx_2x_3x$ spectrum in the degenerate limit $\omega_3 = \omega_2$), is interpreted in an analogous fashion. Here, two peaks at $\omega_t = 0$ appear at oppositely-signed frequencies $\omega_\tau = + \omega_1$ and $\omega_\tau = - \omega_1$ to indicate a rectified response while a single peak appears at $\omega_t = 2\omega_1$ and $\omega_\tau = + \omega_1$ due to second-harmonic generation of a single frequency.

The peak patterns of the two lowest-order coupling terms considered here may be straightforwardly generalized to other possible coupling mechanisms in quantum materials. For example, recent experiments have demonstrated 2DTS as an incisive probe of 'activated' coupling involving phonons[27], magnons[29], and even between magnons and phonons[64]. Higher-order coupling terms[65] should provide even more distinct signatures in 2-D spectra while other more exotic coupling mechanisms (not expected from straightforward symmetry considerations[66]) will also be interesting directions of future studies.

Quantum treatment of 2DTS

In the classical treatment of 2DTS applied above, potential anharmonicities result in six third-order nonlinearities (catalogued in Table 1). These classical nonlinearities each possess direct counterparts in a quantum treatment of 2DTS (applicable, in particular, to fermionic[23] and fractional excitations[56,57]), which is applied ubiquitously to describe multidimensional spectroscopies at higher energy scales (mid-infrared[12] to optical frequencies[14]). In the following, we present a quantum description of 2DTS in qualitative terms to highlight important differences from the classical picture, and leave a detailed discussion of the formalism to more complete texts[12,13,67].

A quantum description of 2DTS typically begins with the optical Bloch equations[68] for the density matrix ρ of a quantum level system. A perturbative solution of the equations[67] then yields an expansion of the density matrix,

$$\rho(t) = \rho^{(0)}(t) + \sum_{n=1}^{\infty} \rho^{(n)}(t), \qquad (7)$$

where the nth order density matrix $\rho^{(n)}$ involves a corresponding number of time-ordered field interactions that each induces a transition in the Bra or Ket of $\rho^{(n)}$. Each sequence of n density matrix elements induced by is commonly referred to as a *quantum pathway*, and possible quantum pathways are conveniently catalogued using so-called double-sided Feynman diagrams.

To construct such diagrams, one begins with an initial density matrix (here we assume a ground state population $|0\rangle\langle0|$) that interacts with the first excitation field. An arrow pointing to the (left)right represents excitation by $E^{(*)}$, while an arrow on the (left)right side of the diagram interacts with the (Ket)Bra of the density matrix. An arrow pointing (into)out of the diagram then results in a transition to a (higher)lower energy level, a consequence of the rotating-wave approximation. The resultant density matrix element evolves along the corresponding experimental time delay - coherences oscillate at the frequency difference of the two states involved, while
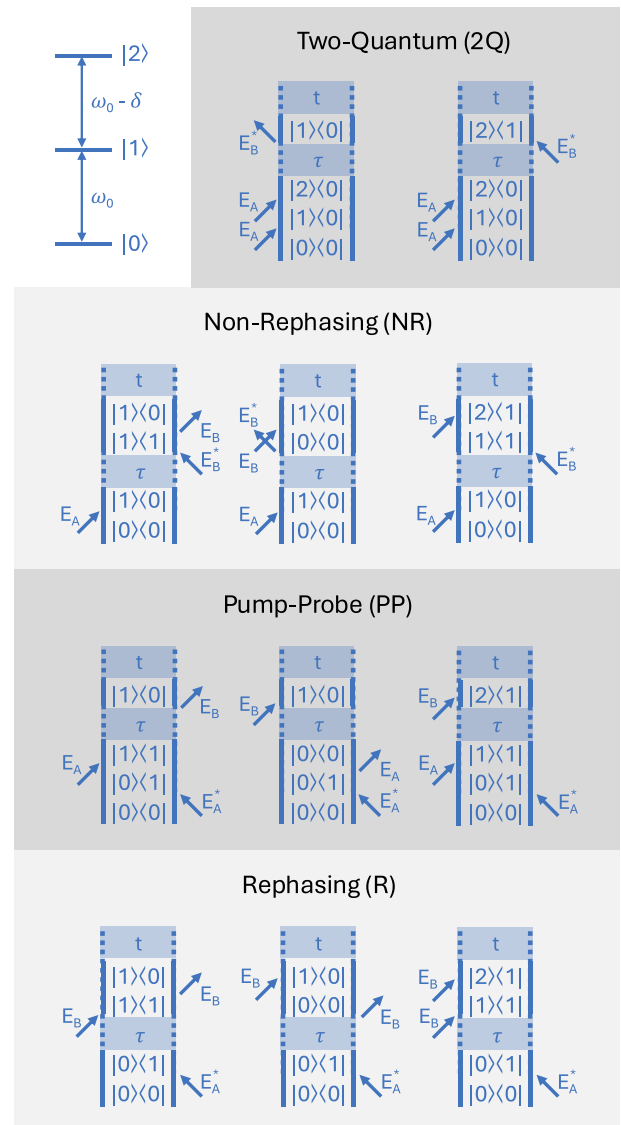

Fig. 4 | Quantum view of two-dimensional terahertz spectroscopy. Double-sided Feynman diagrams describing possible optical nonlinearities for the three-level ladder system shown. Diagrams are constructed according to the rules detailed in the main text, assuming an initial density matrix $|0\rangle\langle0|$. In the case of two-pulse excitation, each pulse may act either once or twice (contribute one or two field interactions) prior to the time delays τ and t as indicated.

populations decay according to their relaxation pathways. Dephasing of coherences can then be included either phenomenologically[12,13] or with a microscopically-motivated spectral density[69,70].

The third-order diagrams for a ladder system comprised of a ground state $|0\rangle$, singly-excited state $|1\rangle$, and doubly-excited state $|2\rangle$ are plotted in Fig. 4, which can be categorized identically to the classical treatment above according to their electric field scaling and frequency coordinates in Table 1. Despite their remarkable similarity, however, we now remark on two important differences between the quantum and classical pictures. (1) The strength of each diagram in Fig. 4 is determined by the product of four dipole moments associated with each density matrix transition (including radiation along the time delay t). One therefore finds that the strengths of the pump-probe, non-rephasing, and rephasing diagrams are identical in the quantum picture, in contrast to their unequal strengths in the classical picture shown in Fig. 1d. (2) Each diagram has a (negative)positive sign for an (odd)even number of arrows on its right side. The two diagrams contributing to the two-quantum nonlinearity are therefore of opposite polarity

Fig. 5 | Pump-2DTS probe spectroscopy of a hypothetical non-equilibrium phase transition. Evolution of the nonlinear optical response is shown as a function of pump-2DTS probe delay t_{p-p}. Before arrival of the pump pulse ($t_{p-p} < 0$), the system is unordered at thermal equilibrium and no rephasing nonlinearity is observed at the salient collective mode frequency ω_0. Upon arrival of the pump pulse E_{pump} ($t_{p-p} = 0$), a non-equilibrium phase transition is initiated. At short timescales ($t_{p-p} > 0$) the non-equilibrium phase is disordered, reflected by an elongated peak in the rephasing 2-D spectrum. At long timescales ($t_{p-p} \gg 0$), the disorder resolves and the rephasing 2-D spectrum becomes correspondingly symmetric.
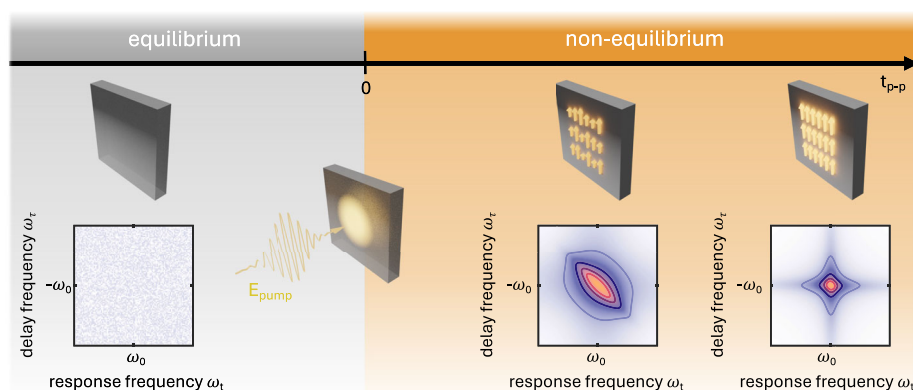
2DTS of quantum materials: out of equilibrium

So far we have considered quantum materials in thermodynamic equilibrium, in which a multitude of quantum phases can be realized by varying *static* parameters such as temperature, pressure, and composition. In contrast to these traditional methods, recent years have witnessed rapid progress in *dynamic* manipulation of quantum materials with light[73]. Light-induced ferroelectricity[74,75], magnetism[76,77], topological switching[78–80], and even putative superconductivity[81–83] are all examples of non-thermal phases that can emerge when quantum materials are pushed out of equilibrium[84]. Below, we provide an outlook for applying 2DTS toward understanding these light-induced phases, as well as the complex interplay of numerous degrees of freedom that underlie many of these spectacular effects.

Pump-2DTS probe experiments

In most demonstrations of light-induced phenomena, an initial 'pump' pulse drives a system into a non-equilibrium state, which is then interrogated by a subsequent 'probe' pulse that measures a one-dimensional (either linear or nonlinear) observable. In this language, one may generalize 2DTS as a multidimensional probe of transient states that measures its multidimensional nonlinear optical response.

We illustrate this idea for a hypothetical light-induced phase transition induced by a pump pulse E_{pump}, in which the final non-equilibrium phase percolates from an initial disordered phase at short timescales. Such ultrafast disorder can then be probed by the rephasing nonlinearity generated by a subsequent 2DTS pulse sequence resonant with a salient collective mode frequency ω_0 (whether phononic, magnetic, superconducting, or otherwise), illustrated in Fig. 5 for increasing values of the pump-2DTS probe time-delay t_{p-p}. Prior to arrival of the pump pulse ($t_{p-p} < 0$), no ordered phase exists at thermal equilibrium and a rephasing nonlinearity is absent for the collective mode that heralds a non-equilibrium ordered phase. Immediately after excitation by the pump pulse ($t_{p-p} > 0$), a non-equilibrium phase forms whose disorder (and that of its concomitant collective mode) is reflected by an elongated rephasing 2-D spectrum[34,54]. With further increasing t_{p-p}, the non-equilibrium phase becomes less disordered and the rephasing 2-D spectrum becomes correspondingly symmetric. We remark that this methodology can only be applied to non-equilibrium states that persist for times long enough for each time delay to be varied in the 2DTS probe[74,77,85,86].

Besides the rephasing nonlinearity, the other nonlinearities measured by 2DTS can provide even more information on non-equilibrium phenomena. For example, the pump-probe nonlinearity can isolate thermal effects such as the melting of competing orders[81,87] while the two-quantum nonlinearity (and its higher-order counterparts) can inform the build-up of non-thermal correlations[88] or loss thereof. Taken together, the information revealed by a 2DTS probe should ultimately address fundamental questions about non-equilibrium phase transitions such as their dynamic universality classes and scaling[89], or whether these equilibrium concepts even apply at all to such radically different timescales.

Perturbative pump experiments

In our final generalization of 2DTS in a non-equilibrium context, we incorporate the 'pump' into part of the 2DTS excitation sequence. In contrast to the typical intense pump field that induces drastic changes in material properties (an overtly non-perturbative response), we consider relatively weak pump fields and an induced response that is perturbative. In this regime the microscopic mechanisms leading to light-induced non-equilibrium phenomena, more specifically the various coupling pathways between a driven mode and other material degrees of freedom, can be characterized.

A recent study reported by Taherian et al.[90] demonstrates the power of this methodology towards studying the underlying mechanism of the light-induced state of underdoped $YBa_2Cu_3O_{6+x}$, in which the appearance of a Josephson plasma edge upon optical excitation was attributed to formation of a non-equilibrium superconducting state. In these experiments, E_A and E_B were tuned to the closely-spaced apical oxygen phonon modes at 17 THz and 20 THz while the nonlinear observable was transient second-harmonic generation induced by the excitation fields[91]. The resultant 2-D spectra revealed unambiguous signatures of Josephson plasma currents cooperatively excited by both driven phonon modes, identified by the characteristic peak pattern of a difference-frequency generation process shown in Fig. 3.

Many other light-induced phenomena result from intricate underlying mechanisms ambiguous to conventional one-dimensional probes. Non-equilibrium superconducting-like states in organic solids[82,92], ferroelectricity in $SrTiO_3$[17,74], and magnetism in $YTiO_3$[77] are all problems that may require a multidimensional probe to disentangle. The additional frequency dimension in 2-D spectra also provides a more efficient alternative for characterizing pump frequency resonances, typically performed in the frequency-domain by sweeping the excitation frequency[93,94].

Outlook

In this Perspective, we introduced the emerging technique of two-dimensional terahertz spectroscopy as an incisive probe of quantum materials, both in and out of equilibrium. Future directions are numerous, but we conclude with three potential developments of particular interest to us.

(1) The coherent nature of 2DTS resolves both the real (dispersive) and imaginary (dissipative) components of the nonlinear optical response[95], information which is typically discarded in most experiments thus far that analyze amplitude 2-D spectra. Developing the experimental and theoretical

framework for analyzing complex 2-D spectra should connect nonlinear observables with their more familiar linear counterparts (optical conductivity, refractive index, etc.), and may even provide insight into the phase of an underlying many-body wavefunction in materials with topological order[96].

(2) Extending scanning probes[97] to perform 2DTS with nanometer resolution and below is another frontier that combines the advantages of multidimensional spectroscopy with imaging capability[98]. Directly correlating the spectral disorder measured by 2DTS with underlying spatial disorder will strengthen the crucial connection between material inhomogeneities and the resultant optoelectronic properties[99].

(3) Finally, 2DTS may also be implemented with ultrafast circuitry[100,101] to reach frequencies below what is possible with free-space optical methods[102]. Such on-chip methods also circumvent the restrictive diffraction limit of terahertz light, and integrate naturally with studies of van der Waals materials and their devices[103,104].

References

1. Keimer, B. & Moore, J. E. The physics of quantum materials. *Nat. Phys.* **13**, 1045–1055 (2017).
2. Tokura, Y., Kawasaki, M. & Nagaosa, N. Emergent functions of quantum materials. *Nat. Phys.* **13**, 1056–1068 (2017).
3. Basov, D. N., Averitt, R. D. & Hsieh, D. Towards properties on demand in quantum materials. *Nat. Mater.* **16**, 1077–1088 (2017).
4. Nicoletti, D. & Cavalleri, A. Nonlinear light–matter interaction at terahertz frequencies. *Adv. Opt. Photon.* **8**, 401–464 (2016).
5. Yang, C.-J., Li, J., Fiebig, M. & Pal, S. Terahertz control of many-body dynamics in quantum materials. *Nat. Rev. Mater.* **8**, 518–532 (2023).
6. Davies, G. & Linfield, E. Bridging the terahertz gap. *Phys. World* **17**, 37 (2004).
7. Kato, Y. D. et al. Optical anomalous hall effect enhanced by flat bands in ferromagnetic van der waals semimetal. *npj Quantum Mater.* **7**, 73 (2022).
8. Okamura, Y. et al. Terahertz lattice and charge dynamics in ferroelectric semiconductor snxpb1-xte. *npj Quantum Mater.* **7**, 91 (2022).
9. Kim, J. et al. Spin and lattice dynamics of the two-dimensional van der waals ferromagnet cri3. *npj Quantum Mater.* **9**, 55 (2024).
10. Friebolin, H. *Basic One- and Two-dimensional NMR Spectroscopy* (VCH, 1991). https://books.google.ch/books?id=cOtqAAAAMAAJ.
11. Keeler, J. *Understanding NMR Spectroscopy* (Wiley, 2010).
12. Hamm, P. & Zanni, M. *Concepts and Methods of 2D Infrared Spectroscopy* (Cambridge University Press, Cambridge, 2012).
13. Li, H., Lomsadze, B., Moody, G., Smallwood, C. & Cundiff, S. *Optical Multidimensional Coherent Spectroscopy* (Oxford University Press, Oxford, 2023).
14. Cundiff, S. T. & Mukamel, S. Optical multidimensional coherent spectroscopy. *Phys. Today* **66**, 44–49 (2013).
15. Fuller, F. D. & Ogilvie, J. P. Experimental implementations of two-dimensional fourier transform electronic spectroscopy. *Annu. Rev. Phys. Chem.* **66**, 667–690 (2015).
16. Liu, A., Almeida, D. B., Padilha, L. A. & Cundiff, S. T. Perspective: multi-dimensional coherent spectroscopy of perovskite nanocrystals. *J. Phys.: Mater.* **5**, 021002 (2022).
17. Lu, J. et al. *Two-Dimensional Spectroscopy at Terahertz Frequencies*, 275–320 (Springer International Publishing, Cham, 2019). https://doi.org/10.1007/978-3-030-02478-9_7.
18. Kuehn, W., Reimann, K., Woerner, M. & Elsaesser, T. Phase-resolved two-dimensional spectroscopy based on collinear n-wave mixing in the ultrafast time domain. *J. Chem. Phys.* **130**, 164503 (2009).
19. Lu, J. et al. Nonlinear two-dimensional terahertz photon echo and rotational spectroscopy in the gas phase. *Proc. Natl Acad. Sci.* **113**, 11800–11805 (2016).
20. Maag, T. et al. Coherent cyclotron motion beyond kohn's theorem. *Nat. Phys.* **12**, 119–123 (2016).
21. Johnson, C. L., Knighton, B. E. & Johnson, J. A. Distinguishing nonlinear terahertz excitation pathways with two-dimensional spectroscopy. *Phys. Rev. Lett.* **122**, 073901 (2019).
22. Houver, S., Huber, L., Savoini, M., Abreu, E. & Johnson, S. L. 2d thz spectroscopic investigation of ballistic conduction-band electron dynamics in insb. *Opt. Express* **27**, 10854–10865 (2019).
23. Mahmood, F., Chaudhuri, D., Gopalakrishnan, S., Nandkishore, R. & Armitage, N. P. Observation of a marginal fermi glass. *Nat. Phys.* **17**, 627–631 (2021).
24. Pal, S. et al. Origin of terahertz soft-mode nonlinearities in ferroelectric perovskites. *Phys. Rev. X* **11**, 021023 (2021).
25. Lin, H.-W., Mead, G. & Blake, G. A. Mapping linbo3 phonon-polariton nonlinearities with 2d thz-thz-raman spectroscopy. *Phys. Rev. Lett.* **129**, 207401 (2022).
26. Luo, L. et al. Quantum coherence tomography of light-controlled superconductivity. *Nat. Phys.* **19**, 201–209 (2023).
27. Blank, T. G. H. et al. Two-dimensional terahertz spectroscopy of nonlinear phononics in the topological insulator mnbi2te4. *Phys. Rev. Lett.* **131**, 026902 (2023).
28. Liu, A. et al. Probing inhomogeneous cuprate superconductivity by terahertz josephson echo spectroscopy. *Nat. Phys.* **20**, 1751–1756 (2024).
29. Zhang, Z. et al. Terahertz-field-driven magnon upconversion in an antiferromagnet. *Nat. Phys.* https://doi.org/10.1038/s41567-023-02350-7 (2024).
30. Katsumi, K. et al. Revealing novel aspects of light-matter coupling by terahertz two-dimensional coherent spectroscopy: The case of the amplitude mode in superconductors. *Phys. Rev. Lett.* **132**, 256903 (2024).
31. Bao, C., Tang, P., Sun, D. & Zhou, S. Light-induced emergent phenomena in 2d materials and topological materials. *Nat. Rev. Phys.* **4**, 33–48 (2022).
32. Gabriele, F., Castellani, C. & Benfatto, L. Generalized plasma waves in layered superconductors: A unified approach. *Phys. Rev. Res.* **4**, 023112 (2022).
33. Fiore, J. et al. Investigating josephson plasmons in layered cuprates via nonlinear terahertz spectroscopy. *Phys. Rev. B* **110**, L060504 (2024).
34. Gómez Salvador, A. et al. Principles of two-dimensional terahertz spectroscopy of collective excitations: The case of josephson plasmons in layered superconductors. *Phys. Rev. B* **110**, 094514 (2024).
35. Strogatz, S. *Nonlinear Dynamics and Chaos* (CRC Press, Boca Raton, 2024).
36. Liu, A. & Disa, A. Excitation-dependent features and artifacts in 2-d terahertz spectroscopy. *Opt. Express* **32**, 28160–28168 (2024).
37. Rajasekaran, S. et al. Parametric amplification of a superconducting plasma wave. *Nat. Phys.* **12**, 1012–1016 (2016).
38. Kim, J., Mukamel, S. & Scholes, G. D. Two-dimensional electronic double-quantum coherence spectroscopy. *Acc. Chem. Res.* **42**, 1375–1384 (2009).
39. Lu, J. et al. Coherent two-dimensional terahertz magnetic resonance spectroscopy of collective spin waves. *Phys. Rev. Lett.* **118**, 207204 (2017).
40. Huang, C. et al. Extreme terahertz magnon multiplication induced by resonant magnetic pulse pairs. *Nat. Commun.* **15**, 3214 (2024).
41. Fulmer, E. C., Mukherjee, P., Krummel, A. T. & Zanni, M. T. A pulse sequence for directly measuring the anharmonicities of coupled vibrations: Two-quantum two-dimensional infrared spectroscopy. *J. Chem. Phys.* **120**, 8067–8078 (2004).

42. Wortis, M. Bound states of two spin waves in the heisenberg ferromagnet. *Phys. Rev.* **132**, 85–97 (1963).

43. Cohen, M. H. & Ruvalds, J. Two-phonon bound states. *Phys. Rev. Lett.* **23**, 1378–1381 (1969).

44. Khalil, M., Demirdöven, N. & Tokmakoff, A. Coherent 2d ir spectroscopy: molecular structure and dynamics in solution. *J. Phys. Chem. A* **107**, 5258–5279 (2003).

45. Gabriele, F., Udina, M. & Benfatto, L. Non-linear terahertz driving of plasma waves in layered cuprates. *Nat. Commun.* **12**, 752 (2021).

46. Klemens, P. G. Anharmonic decay of optical phonons. *Phys. Rev.* **148**, 845–848 (1966).

47. Pirro, P., Vasyuchka, V. I., Serga, A. A. & Hillebrands, B. Advances in coherent magnonics. *Nat. Rev. Mater.* **6**, 1114–1135 (2021).

48. Kim, M.-J. et al. Tracing the dynamics of superconducting order via transient terahertz third-harmonic generation. *Sci. Adv.* **10**, eadi7598 (2024).

49. Puviani, M., Haenel, R. & Manske, D. Quench-drive spectroscopy and high-harmonic generation in bcs superconductors. *Phys. Rev. B* **107**, 094501 (2023).

50. Folpini, G. et al. Strong local-field enhancement of the nonlinear soft-mode response in a molecular crystal. *Phys. Rev. Lett.* **119**, 097404 (2017).

51. Barbalas, D. et al. Energy relaxation and dynamics in the correlated metal sr_2ruo_4 via thz two-dimensional coherent spectroscopy. https://arxiv.org/abs/2312.13502 (2023).

52. Abella, I. D., Kurnit, N. A. & Hartmann, S. R. Photon echoes. *Phys. Rev.* **141**, 391–406 (1966).

53. Hahn, E. L. Spin echoes. *Phys. Rev.* **80**, 580–594 (1950).

54. Siemens, M. E., Moody, G., Li, H., Bristow, A. D. & Cundiff, S. T. Resonance lineshapes in two-dimensional fourier transform spectroscopy. *Opt. Express* **18**, 17699–17708 (2010).

55. Liu, A., Cundiff, S. T., Almeida, D. B. & Ulbricht, R. Spectral broadening and ultrafast dynamics of a nitrogen-vacancy center ensemble in diamond. *Mater. Quantum Technol.* **1**, 025002 (2021).

56. Wan, Y. & Armitage, N. P. Resolving continua of fractional excitations by spinon echo in thz 2d coherent spectroscopy. *Phys. Rev. Lett.* **122**, 257401 (2019).

57. Li, Z.-L., Oshikawa, M. & Wan, Y. Photon echo from lensing of fractional excitations in tomonaga-luttinger spin liquid. *Phys. Rev. X* **11**, 031035 (2021).

58. Kohn, W. Cyclotron resonance and de haas-van alphen oscillations of an interacting electron gas. *Phys. Rev.* **123**, 1242–1244 (1961).

59. von Hoegen, A., Mankowsky, R., Fechner, M., Först, M. & Cavalleri, A. Probing the interatomic potential of solids with strong-field nonlinear phononics. *Nature* **555**, 79–82 (2018).

60. Först, M., Mankowsky, R. & Cavalleri, A. Mode-selective control of the crystal lattice. *Acc. Chem. Res.* **48**, 380–387 (2015).

61. Först, M. et al. Nonlinear phononics as an ultrafast route to lattice control. *Nat. Phys.* **7**, 854–856 (2011).

62. Juraschek, D. M., Fechner, M. & Spaldin, N. A. Ultrafast structure switching through nonlinear phononics. *Phys. Rev. Lett.* **118**, 054101 (2017).

63. Zhang, Z. et al. Terahertz field-induced nonlinear coupling of two magnon modes in an antiferromagnet. *Nat. Phys.* **20**, 801–806 (2024).

64. Mashkovich, E. A. et al. Terahertz light–driven coupling of antiferromagnetic spins to lattice. *Science* **374**, 1608–1611 (2021).

65. Fechner, M. et al. Quenched lattice fluctuations in optically driven srtio3. *Nat. Mater.* **23**, 363–368 (2024).

66. Khalsa, G., Benedek, N. A. & Moses, J. Ultrafast control of material optical properties via the infrared resonant raman effect. *Phys. Rev. X* **11**, 021067 (2021).

67. Mukamel, S. *Principles of Nonlinear Optical Spectroscopy* (Oxford University Press, Oxford, 1999).

68. Cohen-Tannoudji, C., Dupont-Roc, J. & Grynberg, G. *Atom—Photon Interactions: Basic Process and Appilcations* (Wiley, 1998).

69. Liu, A., Almeida, D. B., Bae, W.-K., Padilha, L. A. & Cundiff, S. T. Simultaneous existence of confined and delocalized vibrational modes in colloidal quantum dots. *J. Phys. Chem. Lett.* **10**, 6144–6150 (2019).

70. Liu, A. An exact expression for multidimensional spectroscopy of a spin-boson hamiltonian. *Adv. Quantum Technol.* **7**, 2300399 (2024).

71. Shacklette, J. M. & Cundiff, S. T. Role of excitation-induced shift in the coherent optical response of semiconductors. *Phys. Rev. B* **66**, 045309 (2002).

72. Wang, H. et al. Transient nonlinear optical response from excitation induced dephasing in gaas. *Phys. Rev. Lett.* **71**, 1261–1264 (1993).

73. Disa, A. S., Nova, T. F. & Cavalleri, A. Engineering crystal structures with light. *Nat. Phys.* **17**, 1087–1092 (2021).

74. Nova, T. F., Disa, A. S., Fechner, M. & Cavalleri, A. Metastable ferroelectricity in optically strained srtio₃. *Science* **364**, 1075–1079 (2019).

75. Li, X. et al. Terahertz field–induced ferroelectricity in quantum paraelectric srtio₃. *Science* **364**, 1079–1082 (2019).

76. Wang, X. et al. Light-induced ferromagnetism in moiré superlattices. *Nature* **604**, 468–473 (2022).

77. Disa, A. S. et al. Photo-induced high-temperature ferromagnetism in ytio3. *Nature* **617**, 73–78 (2023).

78. Sie, E. J. et al. An ultrafast symmetry switch in a weyl semimetal. *Nature* **565**, 61–66 (2019).

79. Vaswani, C. et al. Light-driven raman coherence as a nonthermal route to ultrafast topology switching in a dirac semimetal. *Phys. Rev. X* **10**, 021013 (2020).

80. Luo, L. et al. A light-induced phononic symmetry switch and giant dissipationless topological photocurrent in zrte5. *Nat. Mater.* **20**, 329–334 (2021).

81. Fausti, D. et al. Light-induced superconductivity in a stripe-ordered cuprate. *Science* **331**, 189–191 (2011).

82. Mitrano, M. et al. Possible light-induced superconductivity in k3c60 at high temperature. *Nature* **530**, 461–464 (2016).

83. Fava, S. et al. Magnetic field expulsion in optically driven yba2cu3o6.48. *Nature* **632**, 75–80 (2024).

84. de la Torre, A. et al. Colloquium: Nonthermal pathways to ultrafast control in quantum materials. *Rev. Mod. Phys.* **93**, 041002 (2021).

85. Budden, M. et al. Evidence for metastable photo-induced superconductivity in k3c60. *Nat. Phys.* **17**, 611–618 (2021).

86. Maklar, J. et al. Coherent light control of a metastable hidden state. *Sci. Adv.* **9**, eadi4661 (2023).

87. Kogar, A. et al. Light-induced charge density wave in late3. *Nat. Phys.* **16**, 159–163 (2020).

88. Turner, D. B. & Nelson, K. A. Coherent measurements of high-order electronic correlations in quantum wells. *Nature* **466**, 1089–1092 (2010).

89. Halperin, B. I. Theory of dynamic critical phenomena. *Phys. Today* **72**, 42–43 (2019).

90. Taherian, N. et al. Squeezed josephson plasmons in driven $yba_2cu_3o_{6+x}$. https://arxiv.org/abs/2401.01115. (2024).

91. von Hoegen, A. et al. Amplification of superconducting fluctuations in driven $yba_2cu_3o_{6+x}$. *Phys. Rev. X* **12**, 031008 (2022).

92. Buzzi, M. et al. Photomolecular high-temperature superconductivity. *Phys. Rev. X* **10**, 031028 (2020).

93. Liu, B. et al. Pump frequency resonances for light-induced incipient superconductivity in $yba_2cu_3o_{6.5}$. *Phys. Rev. X* **10**, 011053 (2020).

94. Rowe, E. et al. Resonant enhancement of photo-induced superconductivity in k3c60. *Nat. Phys.* **19**, 1821–1826 (2023).

95. Li, X., Zhang, T., Borca, C. N. & Cundiff, S. T. Many-body interactions in semiconductors probed by optical two-dimensional fourier transform spectroscopy. *Phys. Rev. Lett.* **96**, 057406 (2006).

96. Ma, Q., Grushin, A. G. & Burch, K. S. Topology and geometry under the nonlinear electromagnetic spotlight. *Nat. Mater.* **20**, 1601–1614 (2021).

97. Cocker, T. L., Jelic, V., Hillenbrand, R. & Hegmann, F. A. Nanoscale terahertz scanning probe microscopy. *Nat. Photonics* **15**, 558–569 (2021).
98. Chen, X. et al. Modern scattering-type scanning near-field optical microscopy for advanced material research. *Adv. Mater.* **31**, 1804774 (2019).
99. Vojta, T. Disorder in quantum many-body systems. *Annu. Rev. Condens. Matter Phys.* **10**, 233–252 (2019).
100. Gallagher, P. et al. Quantum-critical conductivity of the dirac fluid in graphene. *Science* **364**, 158–162 (2019).
101. Wang, E. et al. Superconducting nonlinear transport in optically driven high-temperature k3c60. *Nat. Commun.* **14**, 7233 (2023).
102. Yoshioka, K. et al. On-chip transfer of ultrashort graphene plasmon wave packets using terahertz electronics. *Nat. Electron.* **7**, 537–544 (2024).
103. McIver, J. W. et al. Light-induced anomalous hall effect in graphene. *Nat. Phys.* **16**, 38–41 (2020).
104. Zhao, W. et al. Observation of hydrodynamic plasmons and energy waves in graphene. *Nature* **614**, 688–693 (2023).

Author contributions
A.L. conceived and wrote the paper.

Competing interests
The author declares no competing interests.

Additional information
Correspondence and requests for materials should be addressed to Albert Liu.

Reprints and permissions information is available at http://www.nature.com/reprints

Publisher's note Springer Nature remains neutral with regard to jurisdictional claims in published maps and institutional affiliations.